The Astrophysical Journal Supplement Series, 207:2 (5pp), 2013 July doi:10.1088/0067-0049/207/1/2

DESIGN AND PERFORMANCE OF A LOW-FREQUENCY CROSS-POLARIZED LOG-PERIODIC DIPOLE ANTENNA

K. Sasikumar Raja, C. Kathiravan, R. Ramesh, M. Rajalingam, and Indrajit V. Barve
Indian Institute of Astrophysics, II Block, Koramangala, Bangalore 560 034, India; sasikumar@iiap.res.in
Received 2013 March 20; accepted 2013 May 15; published 2013 June 10

ABSTRACT

We report the design and performance of a cross-polarized log-periodic dipole (CLPD) antenna for observations of polarized radio emission from the solar corona at low frequencies. The measured isolation between the two mutually orthogonal log-periodic dipole antennas was as low as ≈ -43 dBm in the 65–95 MHz range. We carried out observations of the solar corona at 80 MHz with the above CLPD and successfully recorded circularly polarized emission.

Key words: instrumentation: interferometers – instrumentation: polarimeters – magnetic fields – Sun: corona

1. INTRODUCTION

Circularly polarized radio radiation in the very high frequency range (30–300 MHz) can be received/transmitted using helical antennas, conical log-spiral antennas, cross-polarized Yagi-Uda antennas, cross-polarized log-periodic dipole (CLPD) antennas, etc. In situations where wider frequency coverage (10:1 or even more) is required, CLPD antennas are generally used. A CLPD consists of two linearly polarized log-periodic dipole (LPD) antennas (Duhamel & Isbell 1957) fixed to a common axis in a mutually orthogonal fashion. Log-periodic antennas are widely used in the field of radio astronomy, particularly where simultaneous multi-frequency observations of radio emission from the celestial radio sources are required (Erickson & Fisher 1974; Boischot et al. 1980; Maan et al. 2013). For example, in the case of the solar corona, radio emission at different frequencies originates at different levels in the atmosphere. To obtain data on the activities related to a solar flare, which leads to the generation of transient radio emission almost around the same time at different levels in the solar corona, simultaneous multi-frequency observations are required (Ramesh et al. 1998). However, the typical isolation between the two mutually orthogonal LPDs in commercially available CLPDs is less, ≈ -20 dB (Pivnenko 2006). Because of this limit, an understanding of the polarization characteristics of the weak signals from celestial radio sources can be limited. Note that a 90° hybrid is generally used in conjunction with the CLPD and the polarization strength is measured from the difference of the two outputs of the CLPD. The problem here is that the output from either LPD in a CLPD responds to the total intensity also. So, the observer encounters the difficulty of measuring a small difference between two much larger quantities, similar to polarization observations with circular feeds (Thompson et al. 2007). Though dual-polarized antenna designs offering improved isolation have been mentioned in the literature, they are primarily at frequencies >1 GHz (Pivnenko 2006; Tran & Yagoub 2007). Our interest is to observe the polarized radio emission from the solar corona with high accuracy at low frequencies and use it to estimate the solar coronal magnetic field, one of the holy grails in solar astrophysics. The work reported in this paper is a step to realize the above goal. Note that low-frequency radio emission originates from regions of the solar atmosphere where observations in white light and other regions of the electromagnetic spectrum are presently difficult.

2. DESIGN AND FABRICATION OF THE CLPD

A step-by-step procedure for designing an LPD was first described by Carrel (1961). In our efforts to construct a CLPD, we used the inputs mentioned in the above reference and fabricated an LPD. Figure 1 shows the schematic design of an LPD. It can be shown that the apex angle α is related to the length (L_n) of the adjacent arms and the spacing (S_n) between them as (Kraus 1950; Balanis 2005):

$$L_{n+1} = L_n + S_n \tan\alpha. \quad (1)$$

The length of the adjacent arms and the spacing between them follow the relationship:

$$\frac{L_{n+1}}{L_n} = \frac{S_{n+1}}{S_n} = k, \quad (2)$$

where k is a constant. The frequencies (f) at which an LPD has identical performance are related by the following equations:

$$f_n = f_{n+1} \star k \quad (3)$$

$$\log(f_{n+1}) = \log(f_n) + \log(1/k). \quad (4)$$

Using Equation (1) and by fixing the value of α, the length of the adjacent arms and the spacing between them are calculated iteratively. By making use of the optimum design curve of an LPD (Carrel 1961), the directional gain (G) of the LPD can be decided as a function of apex angle (α), inter-arm spacing (S), and the scale factor k. In the present case, parameters were chosen as: $G = 8$ dBi, $\alpha = 21°$, $k = 1.14$, $S_\lambda = S/\lambda = 0.08$. In practice by using the optimum gain curve, we can choose k for a required gain or vice versa. The relationship between the bandwidth or the frequency ratio of an LPD, i.e., $F = f_{max}/f_{min}$ (where f_{max} and f_{min} are the expected maximum and minimum operating frequencies of the LPD) and the design parameters is given by

$$k^N = F$$

$$N = \frac{\log(F)}{\log(k)}, \quad (5)$$

where N is the number of dipoles. Once the values of k and F are decided, the number of possible arms can be obtained using Equation (5).

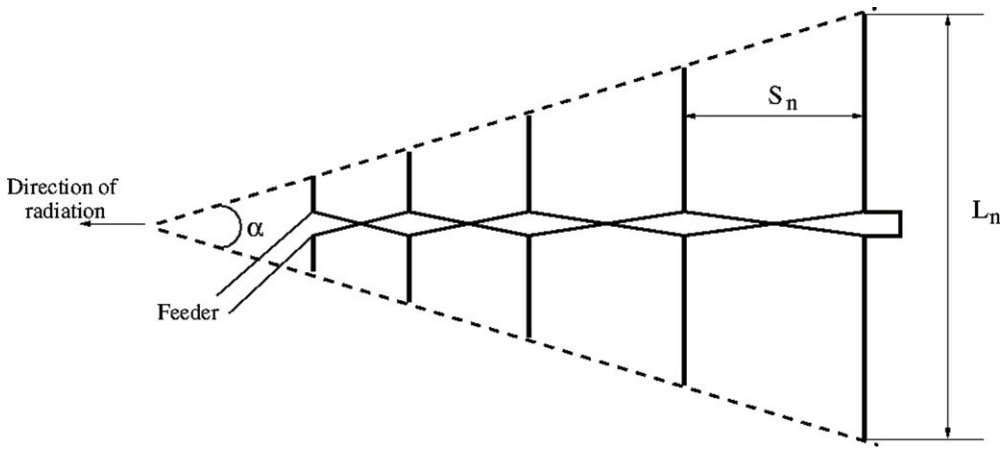

Figure 1. Schematic design of an LPD.

Table 1
Antenna Specifications

S. No.	L_n (cm)	S_n (cm)	Frequency (MHz)
1	79	...	95
2	90	29	83
3	102	31	74
4	116	36	65

Our interest was to design a CLPD for operation in the frequency range ≈65–95 MHz since the existing radioheliograph at the Gauribidanur radio observatory (located about 100 km north of Bangalore in India), where the present work was carried out, operates primarily at 80 MHz (Ramesh et al. 1998, 1999, 2006; Ramesh 2011). The number of arms generally vary with the frequency coverage of the antenna and in the present case it was decided that the LPD be fabricated with four arms, based on the values of F and k mentioned above. The lengths of the different arms of the LPD calculated for the above frequency range are tabulated in Table 1. The arms were designed using commercially available hollow cylindrical aluminum pipes of diameter ≈13 mm and they were fixed (in pairs) to two identical hollow rectangular aluminum pipes (called the booms) separated from each other by a non-conducting spacer in a criss-cross fashion (see Figure 1). The inter-boom separation (D) was calculated using the following equation (Wakabayashi et al. 1999):

$$Z_o = 138 \log_{10}\left(\frac{2\sqrt{2}D}{d}\right), \quad (6)$$

where Z_o is the characteristic impedance of the LPD and d is the width of each boom. We used the commercially available hollow rectangular pipes with $d \approx 2.5$ cm for the boom. We considered $Z_o = 50\Omega$ since the LPD output was tapped using an RF coaxial cable as mentioned below whose characteristic impedance is 50Ω. Substituting the above values in Equation (6), we found that $D \approx 2$ cm. The two booms act like a two-conductor transmission line. They were "shorted" at one of their ends, close to where the arms with the longest length are fixed. The distance between the latter and the "short" (stub) is ≈29 cm. This is one-fourth of the length L_n of the longest arm in the CLPD, i.e., quarter wavelength loop (see Table 1). The output was tapped using an RF coaxial cable connected to the other end of the two booms (close to where the arms with the shortest length are fixed). While the center conductor of the RF coaxial cable was connected to one of the booms, the shield (i.e., the "ground") of the cable was connected to the other boom and the coaxial cable was drawn through the latter as described in Carrel (1961). The "shorting" of the two booms minimizes the impedance mismatch that arises when directly connecting the "unbalanced" RF coaxial cable to the "balanced" LPD. The approximately quarter wavelength of the coaxial cable in the boom acts as a "balun" by presenting a high impedance to any common mode current (Kraus 1950; Balanis 2005). We fabricated two LPDs with the above specifications and combined them in a mutually orthogonal fashion to form a CLPD. We measured the isolation of the CLPD as discussed in Section 3 and found that it is about ≈−20 dBm, nearly the same as that of a commercial CLPD mentioned earlier.

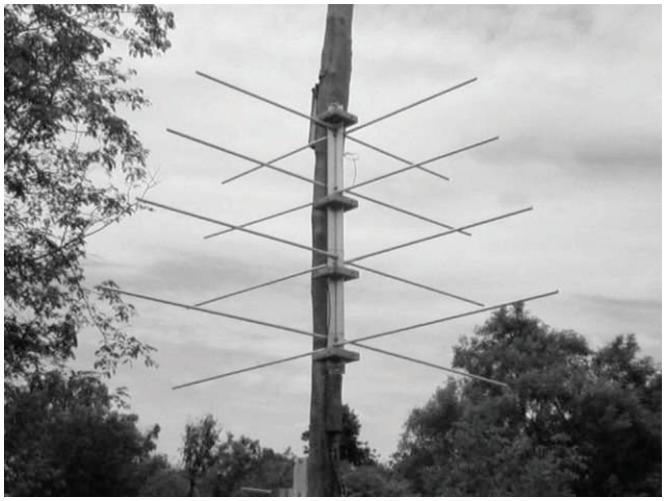

Figure 2. View of the low-frequency CLPD designed and fabricated at the Gauribidanur radio observatory.

It has been suggested that the isolation can be improved by decreasing the inter-boom spacing D to ≈1/100th of the arm length (Pivnenko 2006). So, we designed an LPD/CLPD with $D \approx 5$ mm (smaller than even 1/100th of the shortest arm length in Table 1) using commercially available rectangular aluminum flats as the booms instead of the rectangular hollow aluminum pipes mentioned above. All other specifications including the characteristic impedance were the same. The new CLPD mentioned above is shown in Figure 2. The RF cable was enclosed inside a small aluminum pipe fixed by the side of the

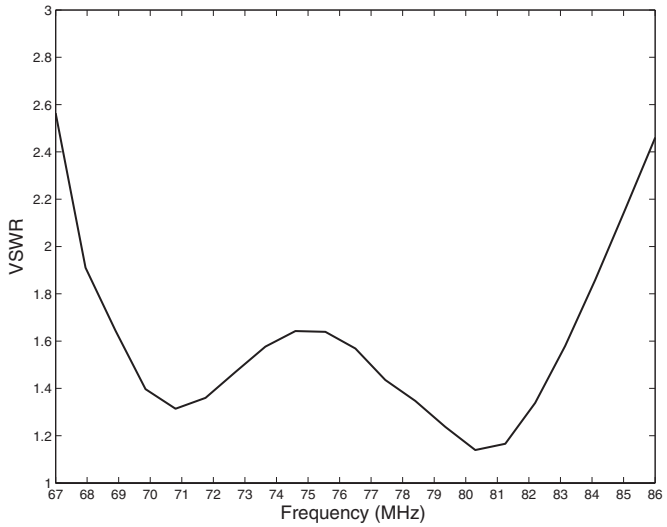

Figure 3. VSWR of the CLPD in Figure 2.

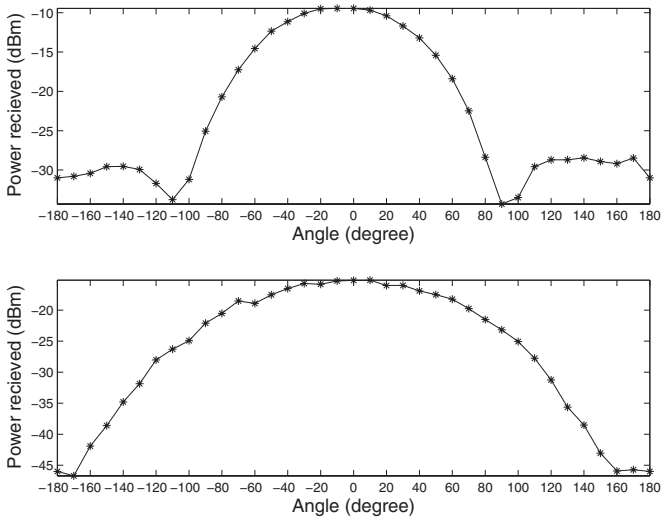

Figure 4. Far field pattern of the CLPD in Figure 2 at 80 MHz. The upper and lower panels correspond to the E-plane and H-plane, respectively.

aluminum flat that was "grounded." The isolation was measured to be < -30 dBm. The details of the isolation and the other measurements carried out with the above CLPD are described in Section 3. Trial observations with the CLPD are mentioned in Section 4.

3. MEASUREMENT OF THE VSWR, ISOLATION AND RADIATION PATTERN OF THE CLPD

3.1. VSWR Measurements

The Voltage Standing Wave Ratio (VSWR) of the LPD/CLPD mentioned above was measured using a vector network analyzer. The values were found to be $\lesssim 2$ for both the LPDs in the frequency range of ≈68–84 MHz (see Figure 3). The VSWR remained nearly the same even after combining the two LPDs to form a CLPD. Due to the radio frequency interference generated by frequency modulation transmissions (88–108 MHz) the higher frequency cutoff in our VSWR measurements were limited to ≈86 MHz.

3.2. Far Field Radiation Pattern Measurements

To measure the far field radiation (Fraunhofer region) pattern, the receiver antenna and the transmitter antenna were mounted on a pole at a height of ≈3 m above the ground level. The antennas were separated by a distance of ≈3 m consistent with the theoretical minimum observation distance for far-field measurements, i.e., $r_{\rm ff} \gtrsim 2l^2/\lambda$, where l is the length of the longest dipole in the CLPD and λ is the wavelength of the transmitted signal (Balanis 2005). At 80 MHz, $r_{\rm ff} \approx 3$ m for $l \approx 2.32$ m (see Table 1). The signal was transmitted using a CLPD and the same was received by the arms of an LPD in the same plane. The measurements were carried out for different angle by rotating the transmitting LPD in the azimuth direction. This corresponds to the E-plane measurement. By mounting the transmitting and the receiving antennas in the vertical direction the measurements were repeated. This corresponds to the H-plane measurement. Figure 4 shows the E-plane and H-plane far field patterns at 80 MHz for the CLPD in Figure 2. The half power beam width (HPBW) in the E-plane and H-plane are $\theta \approx 60^\circ$ and $\phi \approx 120^\circ$, respectively. We repeated the test at different frequencies and found that the E-plane and H-plane widths are similar. The above beam widths correspond to a solid angle, $\Omega = \theta\phi \approx 2.2$ sr. From this we calculated the directional gain of the antenna with respect to an isotropic radiator, i.e., $G = 10\log_{10}(4\pi/\Omega) \approx 7.6$ dBi. The effective collecting area is $A_e = (G/4\pi)\lambda^2 \approx 0.6\lambda^2$. The various parameters of the CLPD are listed in Table 2. One can notice a little asymmetry in the E-plane and H-plane far field patterns in Figure 4. The presence of residual common mode currents could be a reason for this. They may be rejected to a large extent by adding clamp-on ferrite chokes to the coaxial cable. We plan to report this after the commissioning of a larger array with improved version of the CLPD described in the present work.

Table 2
Calculated Parameters of the CLPD in Figure 2

S. No.	Parameter	Value
1	HPBW in the E-plane (θ)	≈60°
2	HPBW in the H-plane (ϕ)	≈120°
3	Solid angle (Ω)	≈2.2 sr
4	Directional gain (G)	≈7.6 dBi
5	Effective collecting area (A_e)	$\approx 0.6\lambda^2$

3.3. Near Field Radiation Pattern Measurements

To obtain the radiating near field (Fresnel region) pattern, we mounted the CLPD on a pole at a height of ≈3 m above the ground level and test (CW) signal was transmitted from one of the LPDs in the CLPD. Using a monopole antenna the signal strength was measured at different distances in the radiating near field range, i.e., $0.62\sqrt{l^3/\lambda} \lesssim r_{\rm nf} \lesssim 2l^2/\lambda$, from the apex of the CLPD and also for different azimuth angles in the range 0°–180°. At 80 MHz, the radiating near field is in the distance range $1\,{\rm m} \lesssim r_{\rm nf} \lesssim 3$ m for $l \approx 2.32$ m (see Table 1). The test was repeated for the same set of distances and angles by transmitting the signal through the other orthogonal LPD. The results were similar. Figure 5 shows the E-plane and H-plane radiating near field patterns at 80 MHz for the CLPD in Figure 2. One can notice that the measured power varies with the distance in the radiating near field range as expected.

3.4. Isolation Measurements

By using the same setup used to measure the far field pattern, we estimated the cross-talk and isolation in the CLPD. The

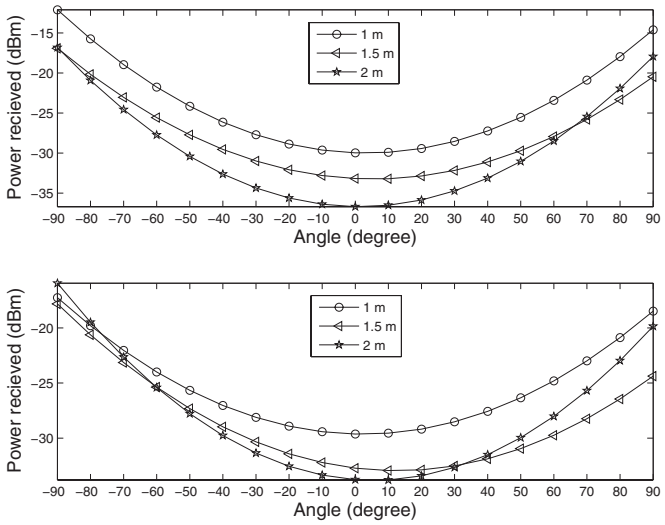

Figure 5. Radiating near field pattern of the CLPD in Figure 2 at 80 MHz. The upper and lower panels correspond to the E-plane and H-plane, respectively. The numbers 1, 1.5, and 2 m in the rectangular box indicate the distances from the apex of the CLPD at which the measurements were obtained.

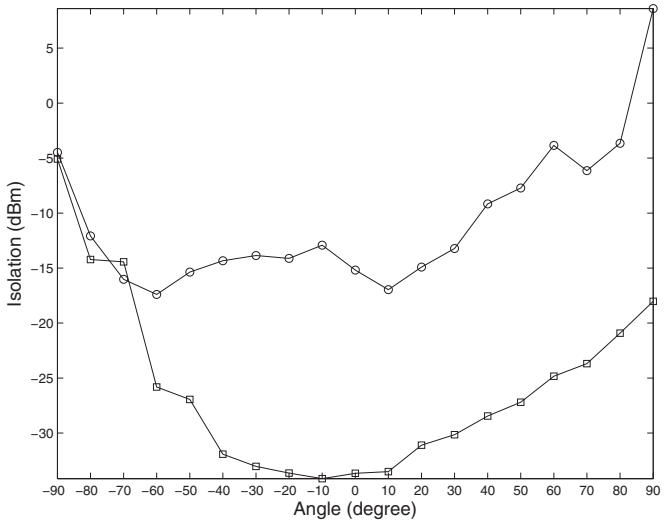

Figure 6. Isolation between the orthogonal LPDs in the CLPD with inter-boom spacing $D = 5$ mm ("squares") and $D = 2$ cm ("circles") at 80 MHz.

transmitting LPD was mounted in the horizontal orientation (0°) and the signal was received by both 0° and 90° oriented arms of the CLPD. In principle, we should receive signal in only the 0° oriented arms of the CLPD. However, a finite signal was received in 90° oriented arms of the CLPD. This is due to the cross-talk between the two orthogonal LPDs in the CLPD. The difference in the signal strength received by the two orthogonal LPDs in the CLPD is a measure of the isolation. The measurements were repeated for different azimuth angles and the results are shown in Figure 6 for a frequency of 80 MHz. The two plots correspond to the CLPD designed with inter-boom spacing (D) of ≈2 cm and ≈5 mm mentioned earlier. While the isolation is ≈−15 dBm for the former, it is <−30 dBm for the latter. The variation of isolation with frequency is shown in Figure 7. We also estimated the isolation in an independent manner by transmitting the CW signal through one of the LPDs in the CLPD in Figure 2 and measuring the received power near the other LPD using a monopole. The results obtained were similar to that in Figure 6. We would like to note here that the isolation bandwidth depends on the extent to which the residual common

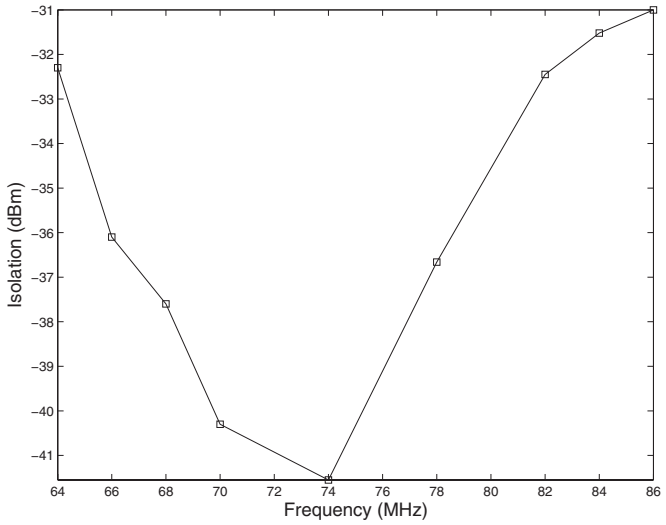

Figure 7. Measured values of isolation (for an azimuthal angle of 0°) at different frequencies for the CLPD in Figure 2 (inter-boom spacing $D = 5$ mm).

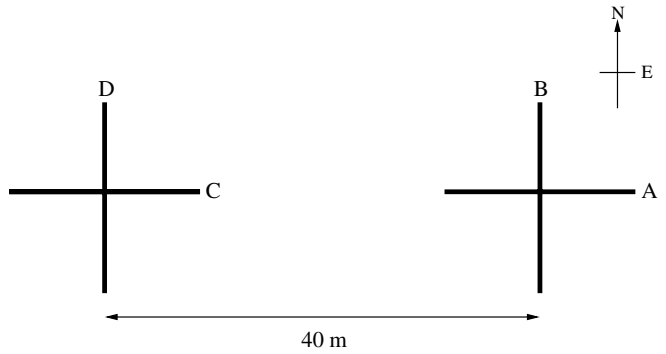

Figure 8. Schematic of the interferometric polarimeter setup using the CLPDs at the Gauribidanur observatory.

mode currents (see Section 3.2) are rejected. It is possible that the limited bandwidth in Figure 7 could be due to the presence of such weak currents in our system.

4. OBSERVATIONS

Two CLPDs similar to Figure 2 were designed and mounted with a separation of ≈40 m in the east–west direction. The CLPDs were at a height of ≈3 m above the ground. They were mounted vertically in such a way that the length of the arms gradually increase from the top to the base. The schematic diagram of the antenna setup is shown in Figure 8. RF output from the LPDs A, B, C, and D was transmitted to a receiver room (about 500 m away) via low loss coaxial transmission lines buried under the ground at a depth of ≈1 m to minimize the phase variations. We operated the setup as a correlation interferometer in the transit mode. The interferometer technique has the advantage of (1) minimizing the contribution from the galactic background radiation and thereby the emission from discrete sources can be observed with better contrast; (2) spurious effects due to ground radiation are less (Morris et al. 1964); and (3) calibration of the observations is also relatively simpler (Weiler 1973; Sault et al. 1996; Ramesh et al. 2008). In Figure 8, the multiplications A × C and B × D respond to the total intensity (Stokes I) and the multiplications B × C and A × D respond to the circularly polarized intensity (Stokes V). In principle the multiplications A × C and B × D record only 50% of the total intensity. Since the situation is the same for

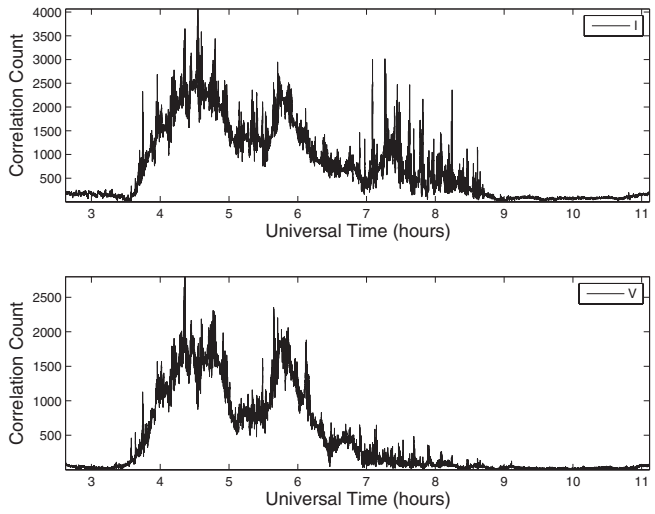

Figure 9. Stokes *I* and *V* emission observed from the solar corona at 80 MHz on 2012 October 5. The top and the lower panel corresponds to Stokes *I* and *V* observations, respectively.

observations on the target as well as the calibrator sources, the error will be minimal. Note that our interest is primarily on observations of the Stokes *V* emission from the solar corona since Stokes *Q* and *U*, which contain information on the linear polarization of the signal, are considered to be extremely small at frequencies $<$100 MHz, particularly over observing bandwidths $\gtrsim$1 MHz. The Faraday rotation of the plane of linear polarization (during transmission through the solar corona and the Earth's ionosphere) is considered to cancel the linear polarization generated at the source when the emission is summed over the observing band (Grognard & McLean 1973). There are reports of observations of high levels of linearly polarized radio emission from the Sun at frequencies $<$100 MHz, specifically over narrow bandwidths in the range $\approx$0.1–10 kHz (Bhonsle & McNarry 1964; Chin et al. 1971). This needs to be verified. We would like to add here that the interferometer method of measuring the Stokes *V* intensity described above differs from the conventional technique where a four-port 90° hybrid is used in conjunction with a crossed dipole feed to extract the Stokes *V* from the difference of the two outputs from the hybrid. This method is also less sensitive to the cross-talk that arises in a hybrid (Cohen 1958). The analog and digital correlator receiver system used for the observations are similar to that described in Ramesh et al. (1998).

We carried out observations of the Sun and a few other unpolarized strong cosmic radio sources (calibrator sources) in both Stokes *I* and *V* using the above setup. The frequency of observation was 80 MHz and the bandwidth was $\approx$1 MHz. Both the Sun and the calibrator sources can be treated as "point" sources since the fringe spacing or the first-null beam width of the interference pattern at the above frequency is broad ($\approx$5°). Figure 9 shows the observations of the circularly polarized radio emission from the Sun on 2012 October 5 with the above setup. The emission is primarily due to the presence of a noise storm source in the solar atmosphere which is known to be circularly polarized (Elgarøy 1977; Ramesh et al. 2011, 2013). Contribution to the Stokes *V* emission from the "undisturbed" background solar corona is expected to be relatively small, particularly at 80 MHz (Sastry 2009). We would like to mention here that the effect of the instrumental circular polarization in our observations can be considered to be very small since the deflection in the Stokes *V* channel while observing some of the strong unpolarized calibrator sources was less than the 3σ level, where σ is the rms noise in the system.

5. SUMMARY

We have reported the design and performance of a CLPD in the frequency range $\approx$68–84 MHz with VSWR $<$ 2 and isolation <-30 dBm between the two mutually orthogonal LPDs that constitute the CLPD. Trial observations indicate that the antennas can be used to effectively observe the circularly polarized radio emission from the solar atmosphere with minimal instrumental polarization. It is possible that the CLPD described can also be used to transmit and receive circularly polarized radio waves in applications involving transmission through the Earth's ionosphere which may produce rotation of the wave polarization (particularly at low frequencies). Note the polarization arriving at the receiver from a linearly polarized transmitting antenna may be practically unpredictable due to reasons mentioned earlier. The compact size of the CLPD described also makes them suitable for use as a primary antenna (feed) that illuminates a parabolic reflector (Smith 2001). We intend to extend the bandwidth of the CLPD and simultaneously observe radio emission from different levels in the solar corona, with an array of CLPDs.

It is a pleasure to thank the staff of the Gauribidanur observatory for their help in the fabrication, testing of the antenna system, and the observations. We also thank the referee for his comments and suggestions to bring out the results of our work more clearly.

REFERENCES

Balanis, C. A. 2005, Antenna Theory: Analysis and Design (New Delhi: John Wiley & Sons)
Bhonsle, R. V., & McNarry, L. R. 1964, ApJ, 139, 1312
Boischot, A., Rosolen, C., Aubier, M. G., et al. 1980, Icar, 253, 399
Carrel, R. 1961, in IRE International Convention Record, Vol., 9, 61
Chin, Y. C., Lusignan, B. B., & Fung, P. C. W. 1971, SoPh, 16, 135
Cohen, M. 1958, PIRE, 46, 172
Duhamel, R. H., & Isbell, D. 1957, in IRE International Convention Record, Vol., 5, 119
Elgarøy, E. Ø. 1977, Solar Noise Storms (London: Pergamon Press)
Erickson, W. C., & Fisher, J. R. 1974, RaSc, 9, 387
Grognard, R. J. M., & McLean, D. J. 1973, SoPh, 29, 149
Kraus, J. D. 1950, Antennas (Singapore: McGraw-Hill)
Maan, Y., Deshpande, A. A., Chandrashekar, V., et al. 2013, ApJS, 204, 12
Morris, D., Radhakrishnan, V., & Seielstad, G. A. 1964, ApJ, 139, 551
Pivnenko, S. 2006, in European Conference on Antennas and Propagation (EuCAP 2006), ed. H. Lacoste & L. Ouwehand (ESA-SP626; France: ESA), 131.1
Ramesh, R. 2011, in Proc. Astron. Soc. India Conf. Ser., Vol. 2, ed. A. R. Choudhuri & D. Banerjee (Bangalore: ASI), 55
Ramesh, R., Kathiravan, C., & Satya Narayanan, A. 2011, ApJ, 734, 39
Ramesh, R., Kathiravan, C., Sundara Rajan, M. S., Barve, I. V., & Sastry, C. V. 2008, SoPh, 253, 319
Ramesh, R., Sasikumar Raja, K., Kathiravan, C., & Satya Narayanan, A. 2013, ApJ, 762, 89
Ramesh, R., Subramanian, K. R., & Sastry, C. V. 1999, A&AS, 139, 179
Ramesh, R., Subramanian, K. R., Sundara Rajan, M. S., & Sastry, C. V. 1998, SoPh, 181, 439
Ramesh, R., Sundara Rajan, M. S., & Sastry, C. V. 2006, ExA, 21, 31
Sastry, C. V. 2009, ApJ, 697, 1934
Sault, R. J., Hamaker, J. P., & Bregman, J. D. 1996, A&AS, 117, 149
Smith, A. A. 2001, Radio Frequency Principles and Applications (Hyderabad: Universities Press)
Thompson, A., Moran, J. M., & Swenson, G. W. 2007, Interferometry and Synthesis in Radio Astronomy (Weinheim: Wiley-VCH)
Tran, A., & Yagoub, M. C. E. 2007, in Progress in Electromagnetics Research Symp. (Cambridge, MA: The Electromagnetics Academy), 30
Wakabayashi, R., Shimada, K., Kawakami, H., & Sato, G. 1999, ITElC, 41, 93
Weiler, K. W. 1973, A&A, 26, 403